FREDI: Robust RSS-based Ranging with Multipath Effect and Radio Interference

Yu Zhao[a], Yunhuai Liu[b], Tingting Yu[a], Chen Qian[c,*]

[a] *University of Kentucky*
[b] *Peking University*
[c] *University of California Santa Cruz*

Abstract

Radio Signal Strength (RSS) based ranging is attractive for mobile device localization due to low cost and easy deployment. In real environments, its accuracy is severely affected by the multipath effect and external radio interference. The well-studied fingerprinting approaches overcome these problems but introduce high overhead in dynamic environments. In this paper, we address the issues using a completely different approach. We propose a new ranging framework called Fredi that exploits the frequency diversity to overcome the multi-path effect solely based on RSS measurements. We design a Discrete Fourier Transformation based algorithm and prove that it has the optimal solution under ideal cases. We further make the algorithm be adaptive and robust to measurement errors and external radio interference which are inevitable in practice. We implement Fredi on top of the USRP-2 platform and conduct extensive real experiments in three different indoor environments. Experimental results show the superiority performance compared to the traditional methods. The ranging errors are consistently less than 0.5m within 4m distance and 1m within 6m distance in dynamic environments, much more accurate than existing solutions using online RSS measures. Other critical factors to influence the accuracy are also discussed and experimented such as the antenna polarization and Huygens

*Corresponding author
Email addresses: yzh355@g.uky.edu (Yu Zhao), yunhuai@pku.edu.cn (Yunhuai Liu), tyu@cs.uky.edu (Tingting Yu), cqian12@ucsc.edu (Chen Qian)

Effect.

Keywords: Ranging, Localization, Frequency Diversity, RSS, DFT.

1. Introduction

Ranging is crucial for precise localization of mobile devices. With an accurate ranging technology, localization can be easily obtained by trilateration [1]. Among various ranging techniques, Radio Signal Strength (RSS) based approaches are attractive due to low cost and easy deployment. Nodes simply measure the pairwise link RSS and then compute the corresponding distance between the sender and receiver.

In an ideal open-space environment, there is a unique monotonic function between RSS and the physical distance which can help to accomplish the computation. In real environments, however, the RSS is severely affected by various physical phenomenon such as the multipath effect and external interference, resulting complex functions of many free parameters. As RSS measurements are the only input during the ranging process, accurate RSS-based ranging is very challenging.

In order to address this issue, a widely studied method is to build a wireless fingerprint map, e.g., RADAR [2] [3]. In these approaches, the system first measures the RSS and constructs an RSS fingerprint for each location. During the ranging process, users refer the corresponding fingerprint to obtain their locations. The main drawback of the fingerprint-based approaches is the excessive overhead. The accuracy of fingerprint-based localization highly depends on fine RSS measurement granularity which may require a lot of measurement efforts. In addition, in mobile networks, environments may change frequently: moving people result in more radio propagation paths and RSS values will vary dramatically. When environmental dynamics happen, the calibrated fingerprints will fail and have to be re-constructed.

Re-visiting the problem, we find that instead of offline calibrations, a more efficient way is to investigate all the affecting factors in an online manner. We

can build an RSS model, taking all the dynamic factors into consideration, and collect enough RSS measurements to figure out the real distance. By this approach, the ranging process is highly adaptive to environments and robust to dynamics.

Towards this end, we need more independent inputs than a single RSS value. Using frequency diversity, a given pair of nodes may have very different RSS values at different frequencies, mainly due to the multipath effect. When there are different paths, waves of different paths will combine constructively or destructively depending on their phases. As the phase is a function of the frequency, the combination of waves will be different at different frequencies, resulting in varied RSS values. By carefully analyzing the differences among these RSS values, we can obtain the phase information, and accordingly compute the distance. For ease of presentation, we name the general framework as Fredi.

By analyzing RSS values, we find that the RSS value model function has a very special structure of trigonometric components (e.g., sine and cosine functions). For such a structure, Discrete Fourier Transformation (DFT) is a powerful tool which is originally used for signal processing. Based on DFT, we design algorithms and prove that in the ideal case, the ranging solutions are accurate. In real environments, these algorithms do not perform well because of the measurement errors and other practical reasons. We therefore design a revised DFT-based algorithm which provides robustness to such errors. The robust algorithm takes approximation and analysis results give a tight bound on the ranging errors introduced by the approximation.

Compared with traditional RSS-based ranging techniques, Fredi mainly exhibits the following advantages. It does not require any special hardware and no physical layer information is needed other than RSS values. The only input is RSS values and the only requirement is the fast frequency hopping, which has been widely used in existing systems. During the ranging process, only the transmitter and receiver are involved and no other cooperation is needed. Fredi is highly adaptive to environments and robust to dynamics. During our experiments people can freely move around. In addition, external radio interference

at certain number of frequencies can be tolerated.

The main contributions of this paper are as follows:

First, to the best of our knowledge, we are the first to address the multi-path effect, measurement errors and radio interference for device ranging solely based on RSS measurements.

Second, we design a novel DFT-based algorithm and prove that the algorithm can produce exact solutions in the ideal case. We further design a robust DFT-based algorithm to tolerate the measurement noises and provide robustness to external interference in real environments. Analytic results give a tight bound on the approximation errors.

Third, we implement the proposed algorithms on top of the USRP2 platform and conduct comprehensive indoor experiments. Results show that in all three indoor environments, the range errors are consistently less than 0.5m within 4m distance and 1m within 6m distance, much more accurate than existing solutions using online RSS measures.

Fourth, we also investigate the limitations of Fredi and demonstrate that antenna polarizations, Huygens effect, and the hardware limitations on the supported frequency are the main sources of the ranging errors.

The rest of the paper will be organized as follows. In Sec. 2, we start from the background of the Fredi ranging including the motivation and the Fredi's framework. In Sec. 3, we show how to solve the problem under the ideal case, and extend the algorithms to more general cases. We give analysis on Fredi in Sec. 6 and conduct performance evaluation in Sec. 7. More practical issues will be discussed in Sec. 8 and in the last section, we draw conclusions and point out future work directions.

2. Background

In this section, we give some background information including the insight of the frequency diversity for RSS-based ranging and Fredi general framework.

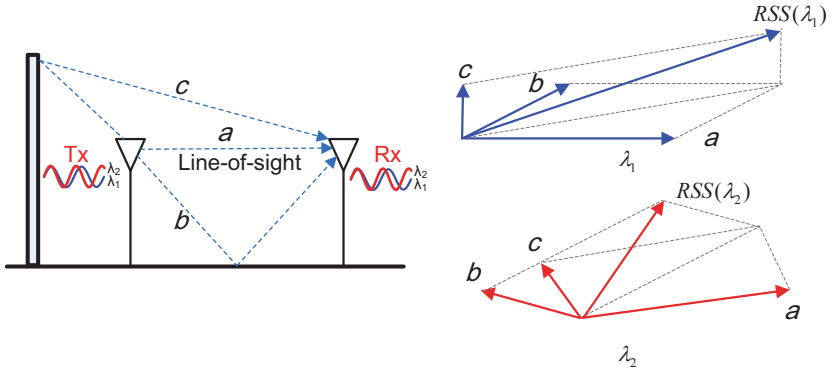

Figure 1: An illustrative example; there are two paths, and the radio waves will combine at Rx, resulting in different RSS values at different frequencies

2.1. Motivation

Fredi is in-sighted by FARA [4], a rate adaption algorithm that exploits frequency diversity to improve wireless communication efficiency. Because of the frequency diversity, a pair of nodes may have very different RSS values at nearby frequencies. Frequency diversity is mainly caused by the multi-path effect in which the radio waves will traverse through different physical paths. Such RSS difference carries the path information, which can be explored to figure out all the dynamic information.

Fig. 1 depicts an illustrative example. Suppose there are two radio paths a and b between the transmitter and the receiver. Waves from each path are featured by two variables, the amplitude, and the phase. At each frequency, because of the different path lengths, there will be a phase difference $\frac{d_a - d_b}{\lambda}$. And at different frequencies, this phase difference will also be different, i.e., $\frac{d_a - d_b}{\lambda_1}$ and $\frac{d_a - d_b}{\lambda_2}$, resulting in changed RSS values. By exploring such different RSS, we can build equations to figure the path length d_a out.

In the next subsection, we give a general framework of Fredi that exploits the frequency diversity for RSS-based ranging.

2.2. Fredi general framework

Fredi ranging has a very simple framework (Fig. 2). Compared with the standard RSS-based ranging, Fredi simply adds one more operation. After

each RSS measurement, the transmitter and receiver should switch to another frequency and collect the new RSS value. As long as all supported frequencies are measured, we can make the computation. Supposing there are N different frequencies, we thus can have up to N RSS measurements, denoted as $\hat{s}_n, n \leq N$. Our goal is to figure out all the dynamic factors that fit these measurements, i.e.,

$$Input : \lambda_n, \hat{s}_n, n \leq N$$
$$Output : d_1$$

where d_1 is the physical distance between the transmitter and receiver. Mathematically this is a curvature fitting problem that belongs to non-linear optimization category. We however find that such problem has no standard methods and needs a customized solution.

In the next we will present our DFT-based solution. To ease the presentation, we will start from analyzing the simplest 1-path scenario, i.e., there is only one radio path between nodes, and gradually approach the ultimate goal, i.e., the general scenario where there are an arbitrary, unknown number of paths, and measurements contain errors and external radio interference. The road map of the algorithm designs is in Tab. 1.

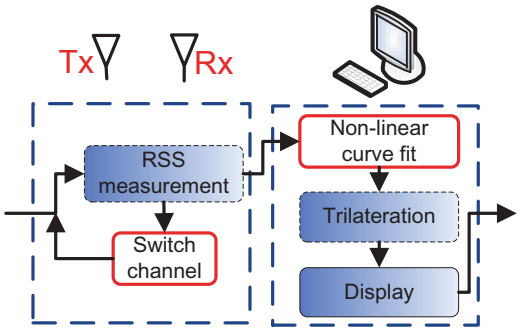

Figure 2: General framework of Fredi

Table 1: Algorithm design road map

Sec.	M=1	M=2	M=3	M is given	M is unknown	With noise
3.1	√	x	x	x	x	x
3.3	√	√	x	x	x	x
3.4	√	√	√	x	x	x
3.5	√	√	√	√	x	x
4.2	√	√	√	√	x	√
4.3	√	√	√	√	√	√

3. Ideal Scenarios

In this section, we present the Fredi algorithm to solve the problem. We start from the simplest 1-path scenario, and extend to two-path, three-path, and finally to the general M-path scenario. In this section, we all assume the number of paths is known and there is no measurement error or radio interference. Some notations used in this paper are listed in Tab. 2

Table 2: Notations

	Description
N	The number of support frequencies, given
M	The number of radio paths, unknown
λ_n	The n-th wavelength, $n \in [1, N]$
d_m	The length of m-th path, d_1 is for the LoS path
Γ_m	The reflection coefficiency of the m-th path, $\Gamma_1 = 1$ is for LoS path and $\Gamma_m < 1, m \in (1, M]$ is for NLoS path
$s(\lambda)$	The RSS model function with respect to the wave length λ
$\hat{s}_n$	The measured RSS at the n-th frequency, $n < N$
ϵ	The fitting error square between $s(\lambda)$ and $\hat{s}_n$
$P(k)$	The DFT transformation sequence of $\hat{s}_n$, $k = 1, ąŋN$
P_i	i-th largest $P(k)$, $P_1 = \max(P(k))$

3.1. One-path Scenario

In the simplest one-path scenario, the solution is quite straightforward. Radio wave propagations follow the physical laws which are the foundation of wireless communications. During the propagations, radio wave energy field will fade out. Consider a simple sine radio wave (more complex waves will be discussed in Sec. 5). When the waves directly propagate to the receiver, a Line-of-sight (LoS) path is established. The LoS path propagations can be modeled by the Friss open space model where the energy field strength is

$$E_{LoS}(t) = \frac{\sqrt{G_t G_r P_t}}{\sqrt{4\pi} d} \sin(\frac{2\pi c}{\lambda} t + 2\pi \frac{d}{\lambda}) \tag{1}$$

Here G_t is the gain of the sender, G_r is the receiver gain, P_t is the transmission power, λ is the radio wavelength, c is the light speed, d is the LoS path length and t is the time. According to Eq. 1, under the single path scenario, the RSS at different frequencies $\hat{s}_n$ is independent of the frequency(Notice that RSS and energy field strength are not same thing, RSS can be computed as below). Thus, the LoS path length d, also the physical distance between the transmitter and receiver, can be easily obtained by

$$\frac{G_t G_r P_t}{8\pi d^2} = \hat{s}_n$$

Here G_t, G_r, P_t are hardware dependent that can be obtained in an offline manner. Since this is a single-run operation, the overhead is acceptable.

3.2. Two-path Scenario

In this part, we first introduce the physical laws of multipath effect, and then derive the system model for the two-path scenario and propose our DFT-based solution.

3.2.1. Multi-path effect

In practical environments, there can be two or more physical radio propagation paths from the transmitter to the receiver, referred to as multi-path

phenomenon. The causes of the multi-path effect are many, such as the atmospheric duct, refraction and reflection. Besides the LoS path, the other physical paths are called Non-Line-of-Sight (NLoS) path.

NLoS paths change in direction of the signal waves at an interface between two different media, resulting in the returned wave to the original medium. In the indoor environments, the reflections typically occur at the surface of the objects, walls, and the ground. With each reflection, partial energy will be the transmittance, partial will be reflected, and the left is absorbed by the medium. An NLoS path will introduce the energy field as

$$E_{NLoS}(t) = \Gamma \frac{\sqrt{G_t G_r P_t}}{\sqrt{4\pi} d} \sin(\frac{2\pi c}{\lambda} t + 2\pi \frac{d}{\lambda}) \tag{2}$$

where $\Gamma \in (0, 1)$ is a reflection coefficient. Refraction is another source of the NLoS paths. It has a similar effect and thus can also be modeled by Eq. (2). Notice that Eq. (2) can also express LoS path with $\Gamma = 1$.

Let d_1 be the LoS path and d_2 the NLoS one. When waves arrive at the receiver through the two paths, the electromagnetic field at receiver is addition of the two fields. Here, the "field" is a vector that is a function of position and time. The RSS (Received signal strength indication) is the time averaged power of the result of addition.

When waves arrive at the receiver through the two paths, their signals will be added, and the RSS is the averaged power of the received signal, i.e., The RSS can be expressed as Eq. (3) at the receiver and the details are at Sec.(10) with $n = 2$.

$$\begin{aligned} s(\lambda) &= C\lambda^2 \sum_{t=1}^{N} \frac{(E_1(t) + E_2(t))^2}{N} \\ &= C\lambda^2 (\frac{1}{2d_1^2} + \frac{\Gamma_2^2}{2d_2^2} + \frac{\Gamma_2}{d_1 d_2} \cos(\frac{d_1 - d_2}{\lambda})) \end{aligned} \tag{3}$$

where $C = \frac{P_t G_t G_r}{480\pi^2}$ is a hardware-dependent constant that can be obtained in an offline manner, E_1 is the energy field of the LoS path and E_2 is of the NLoS

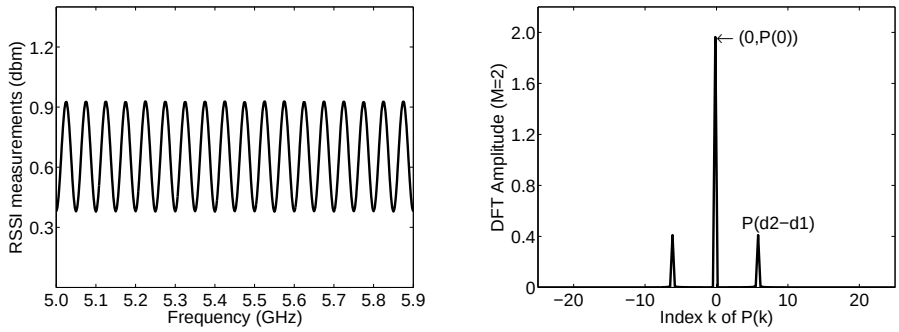

Figure 3: A two-path scenario with $d_1 = 4$, $d_2 = 10$, and $\Gamma = 0.5$, and its DFT amplitudes; there are two non-negative values, $P(0)$ and $P(d_1 - d_2)$

path. As the convention, $s(\lambda)$ in Eq. (3) is called model function.

Fig. 3 gives an example of Eq. (3). This is a typical trigonometric function that exhibits periodical properties. It has the periodical part $\cos(\frac{d_1-d_2}{\lambda})$ that determined by the two path *length difference* d_1-d_2 and the wave length λ. The rational in behind is that the radio waves from the two paths will experience a *phase difference* $\Delta\theta = 2\pi(\frac{d_2-d_1}{\lambda} - \lfloor\frac{d_2-d_1}{\lambda}\rfloor)$. It is determined by the path length difference $d_2 - d_1$ and the radio wave length λ. The value $d_2 - d_1$ will not change, while λ is changing as the frequency changes. As a result, the phase difference $\frac{d_2-d_1}{\lambda}$ will change and exhibit certain periodic property.

For example, let $d_1 = 6m$, $d_2 = 11m$ and the path difference is $d_2-d_1 = 5m$. At 5.01GHz ($\lambda_1 = 0.0599$), the phase difference is

$$\Delta\theta = 2\pi(\frac{5}{\lambda_1} - \left\lfloor\frac{5}{\lambda_1}\right\rfloor) = 2\pi(\frac{5}{0.0599} - \lfloor\frac{5}{0.0599}\rfloor) = \pi$$

The two path waves are destructive. At 5.4G, the phase difference becomes $\Delta\theta = 0$ which is completely constructive. At 5.85G ($\lambda_2 = 0.0513$), it is again $\Delta\theta = 2\pi(\frac{5}{0.0513} - \lfloor\frac{5}{0.0513}\rfloor) = \pi$ and destructive. Indeed, as the frequency scans from 5.01G to 5.85G, the phase difference has been periodically changed for $(\frac{5}{\lambda_1} - \frac{5}{\lambda_2}) = 14$ periods. In the next, we will show how to compute d_1 based on Eq. 3.

3.2.2. DFT-based solution

Fourier analysis is a mathematical tool that helps to find periodic properties of a function. It decomposes the function into its constituent frequencies, and the amplitudes at the frequencies will reflect the periodic strength at the corresponding frequencies. Notice that this "frequency" is not the same frequency of radio waves in wireless communications. Fourier analysis has been widely used in many fields and is particularly useful for functions with trigonometric components like Eq. (3).

Discrete Fourier Transformation (DFT) is a discrete method of Fourier analysis. Given a sequence of N discrete values x_n , DFT transforms them into another sequence of N numbers by the formula [5]:

$$P(k) = \sum_{n=1}^{N} x_n \cdot e^{-i2\pi \frac{k}{N} n}, k = 1, ..., N \tag{4}$$

As $P(k)$ is an even function with respect to k, in the remainder of this paper we consider only the positive part of $P(k)$, i.e., $k > 0$. The $P(0)$ will be explicitly identified besides $P(k)$. We call k the $P(k)$'s index, and $P(k)$ the DFT amplitude indexed by k.

Given a sequence of N discrete values $x_n = \frac{\hat{s}_n}{c \cdot \lambda_n^2}$ and applying Eq. (4) on Eq. (3), we have $P(0) = \frac{1}{2d_1^2} + \frac{\Gamma_2^2}{2d_2^2}$ and $P(d_1 - d_2) = \frac{\Gamma_2}{d_1 d_2}$. Let P_i be the i-th largest DFT amplitude among all $P(k)$, i.e., $P_1 = \max(P(k))$ and so on, and $\arg_k(P_1)$ be the x-axis index of P_1, i.e., $P(\arg_k(P_1)) = P_1$. In two-path cases, there is only one non-zero $P(k)$, and thus $P(d_1 - d_2) = P_1$. As such, we rewrite the equations as

$$\begin{cases} \frac{1}{2d_1^2} + \frac{\Gamma_2^2}{2d_2^2} &= P(0) \\ \frac{\Gamma_2}{d_1 \cdot d_2} &= P_1 \\ d_2 - d_1 &= \arg_k(P_1) \end{cases}$$

Here we have three unknowns d_1, d_2, Γ_2 and three simple equations. The solution is straightforward and omitted.

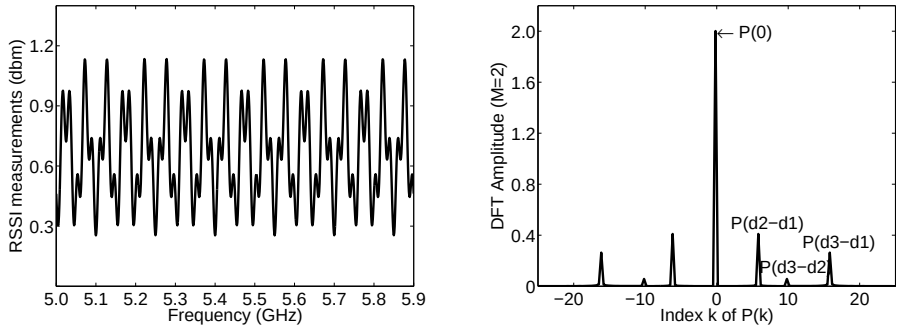

Figure 4: A three-path case with $d_1 = 4$, $d_2 = 10$, $d_3 = 20$, and all $\Gamma = 0.5$, and its DFT amplitudes; there are four non-negative values including $P(0)$

3.3. Three-path case

Three-path cases are more complex than the two-path cases. An example of three-path case measurements and the DFT amplitudes are shown in Fig. 4. When there are three paths, the model function $s(\lambda)$ is

$$\begin{aligned} s(\lambda) &= C\lambda^2 \sum_{t=1}^{N} \frac{\left(E_1(t) + E_2(t) + E_3(t)\right)^2}{N} \\ &= C\lambda^2 \left(\frac{1}{2d_1^2} + \frac{\Gamma_2^2}{2d_2^2} + \frac{\Gamma_3^2}{2d_3^2} + \frac{\Gamma_2}{d_1 d_2}\cos\left(\frac{d_1 - d_2}{\lambda}\right)\right. \\ &\quad \left. + \frac{\Gamma_3}{d_1 d_3}\cos\left(\frac{d_1 - d_3}{\lambda}\right) + \frac{\Gamma_2\Gamma_3}{d_2 d_3}\cos\left(\frac{d_2 - d_3}{\lambda}\right)\right) \end{aligned} \tag{5}$$

Without lose of generality, assume $\frac{\Gamma_2}{d_2} \geq \frac{\Gamma_3}{d_3}$. Applying the DFT method on this model function $s(\lambda)$, we have (indeed, there are more equations but we do not need them in this part)

$$P_1 = \frac{\Gamma_2}{d_1 d_2}, \quad P_2 = \frac{\Gamma_3}{d_1 d_3}, \quad P_3 = \frac{\Gamma_2\Gamma_3}{d_2 d_3} \tag{6}$$

where P_i is the i-th largest $P(k)$. Noticing that

$$\frac{P_3}{P_1 \cdot P_2} = \frac{\Gamma_2\Gamma_3}{d_2 d_3} \Big/ \frac{\Gamma_2}{d_1 d_2} \cdot \frac{\Gamma_3}{d_1 d_3} = d_1^2 \tag{7}$$

and thus $d_1 = \sqrt{P_3/P_1 \cdot P_2}$. Eq. (7) is a foundation of our rest algorithm

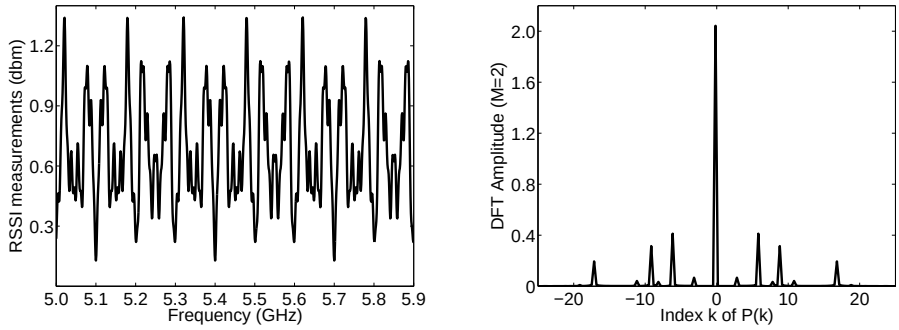

Figure 5: An M-path case with $d_1 = 4, d_2 = 10, d_3 = 13, d_4 = 21, d_5 = 40$, all $\Gamma = 0.5$, and its DFT amplitudes; there are 10 non-negative $P(k)$

design.

3.4. M-path case

Suppose there are an arbitrary number of paths between the transmitter and receiver and this number of paths M is known. In this scenario, we note that Eq. (7) still holds but Eq. (6) does not work because there are many non-zero values and we have no idea which three satisfy Eq. (7). The main tasks of this subsection is then to identify three such DFT amplitudes.

When there are M different paths, the RSS at the receiver can be expressed as (details are at section.10)

$$s(\lambda) = C \cdot \lambda^2 \cdot (\sum_{m=1}^{M} \frac{\Gamma_m}{2d_m^2} + \sum_{m \neq m'} \frac{\Gamma_m \Gamma_{m'}}{d_m d_{m'}} \cos(\frac{d_m - d_{m'}}{\lambda})) \tag{8}$$

where d_m and Γ_m are the m-th path length and reflection coefficient. Applying the DFT method on $s(\lambda)$ we get

$$\begin{cases} P(0) = \sum_{m=1}^{M} \frac{\Gamma_m}{2d_m^2} \\ P(d_m - d_{m'}) = \frac{\Gamma_m \Gamma_{m'}}{d_m d_{m'}} \end{cases} \tag{9}$$

Fig. 5 gives an example of $\hat{s}_n$ and the DFT amplitude $P(k)$ under a 5-path scenario. According to Eq. (9), at each combination of $k = d_m - d_{m'}$, there will be a non-zero value $P(d_m - d_{m'}) = \frac{\Gamma_m \Gamma_{m'}}{d_m d_{m'}}$. In total, there are $\binom{M}{2} = M(M-1)/2$

non-zero $P(k)$. We call $P(d_m - d_{m'})$ the DFT amplitude induced by the d_m and $d_{m'}$ paths. From this number of non-zero P(k) we need to identify three P(k) satisfying that, the former two are respectively induced by the LoS path and a NLoS path, and the last one is induced by the latter two NLoS paths. In other words, the three should have the form as $P(d_1 - d_m)$, $P(d_1 - d_{m'})$, and $P(d_m - d_{m'})$. For this we have,

Lemma 3.1. $\forall m, m' > 1, P(d_1 - d_m) > P(d_{m'} - d_m)$

Proof. Because of its very nature, the LoS path has the largest reflection coefficiency $\Gamma_1 = 1$ and the shortest path length d_1 compared with NLoS paths, i.e., $\forall m > 1$, $\Gamma_1 = 1 > \Gamma_m$ and $d_1 < d_m$. Thus we have $\frac{1}{d_1} > \frac{\Gamma_m}{d_m}$. Applying these two inequations in Eq. (9), we have $\forall m, m' > 1$ $P(d_1 - d_{m'}) = \frac{\Gamma_{m'}}{d_1 d_{m'}} > \frac{\Gamma_m \Gamma_{m'}}{d_m d_{m'}} = P(d_m - d_{m'})$ □

Theorem 3.2. *When $M \geq 3$, the two largest DFT amplitude P_1 and P_2 must be induced by the LoS path and a NLoS path respectively.*

Proof. By Lemma 3.1, P_1 must be induced by the LoS path and an NLoS path. Otherwise, it will be smaller than the amplitude induced by the LoS and NLoS path and cannot be the largest one. Denote this NLoS path as $m1$.

We then prove that P_2 is also induced by LoS path and another NLoS path $m2$. We prove by contradictions. Assume P_2 is induced by two NLoS paths denoted as $P(d_m - d_{m'})$, $d_m, d_{m'} \neq d_1$. By Lemma 3.1, $P(d_1 - d_{m'}) > P(d_m - d_{m'})$. Recalling that $P(d_1 - d_{m1}) > P(d_m - d_{m'})$ and $P(d_m - d_{m'})$ is the second largest one, we have $P(d_1 - d_{m'}) = P(d_1 - d_{m1})$, and thus $d_{m1} = d_{m'}$.

By Eq. (9), we have

$$\begin{aligned} P(d_m - d_{m'}) &= P(d_m - d_{m1}) \\ &= \frac{\Gamma_m \Gamma_{m1}}{d_m d_{m1}} \\ &< \frac{\Gamma_m}{d_m d_1} \\ &= P(d_1 - d_m) \end{aligned} \tag{10}$$

In other words, $P(d_m - d_{m'})$ is less than both $P(d_1 - d_m)$ and $P(d_1 - d_{m1})$, and $P(d_1 - d_m) \neq P(d_1 - d_{m1})$. Thus $P(d_m - d_{m'})$ cannot be P_2. □

With this theorem, the identification of three amplitudes for Equ (7) becomes straightforward. The two largest one DFT amplitude P_1 and P_2 will satisfy the first two, and the third one $P(d_m - d_{m'})$ can be obtained by

$$d_m - d_{m'} = (d_1 - d_{m'}) - (d_1 - d_m) = \arg_k(P_1) - \arg_k(P_2)$$

where $\arg_k(P_i)$ is the index of P_i. Thus, we have

$$d_1 = \sqrt{P(\arg_k(P_1) - \arg_k(P_2))/(P_1 P_2)} \tag{11}$$

Notice that Eq. (11) is an exact express. It will produce optimal solutions when all the input P_1, P_2, and $P(\arg_k(P_1) - \arg_k(P_2)$ are accurate.

4. Robustness and Unknown M

The M-path algorithm in Sec. 3.4 is accurate and simple to adopt. It however may produce large errors when there are measurement errors. The known M is also an impractical assumption. In this section, we will show how to deal with these challenges by proposing a robust M-path algorithm with unknown M.

4.1. Limitations of M-path algorithm

One source of the errors is by the $\hat{s}_n$'s measurement errors. Such errors may be introduced by hardware variations, system errors, or external interference, which is inevitable and will propagate to P_1, P_2, $P(\arg_k(P_1) - \arg_k(P_2))$, and finally to d_1. Notice that Eq. (7) is very sensitive to $P(k)$ values, while $P(\arg_k(P_1) - \arg_k(P_2))$ the M-path algorithm is typically very small and easy to be impaired by noises.

Another important source of the errors is by the so-called *spectral leakage* [6] from DFT method itself. Roughly speaking, DFT processes only discrete

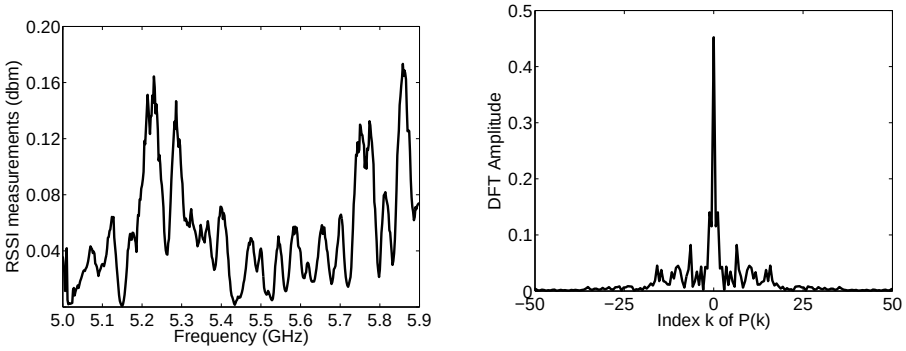

Figure 6: Real measurements of RSS and the DFT amplitudes

values, requiring the index k to be integer. This requirement may not (indeed, often not) be satisfied as $k = d_m - d_{m'}$ is controlled by the path lengths. When $k = d_m - d_{m'}$ is not an integer, $P(d_m - d_{m'})$ will be "leaked" out of $d_m - d_{m'}$ to some nearby integer-indexed $P(k)$.

Figure 6 gives an example of real measured $\hat{s}_n$ and the corresponding $P(k)$.

4.2. Robust M-path algorithm

To be robust to the input errors, a key observation is that the large amplitudes (e.g., P_1, P_2 in Eq. 7 are robust while small values (e.g., $P(\arg_k(P_1) - \arg_k(P_2))$) are more prone to be impacted. Accordingly, in our robust DFT-based algorithm, we prefer to use large $P(k)$, e.g., the largest P_i.

Towards this end, we notice that $\forall m$

$$\frac{\Gamma_m^2}{d_m^2} = \frac{\Gamma_m}{d_1 d_m} \cdot \frac{\Gamma_m}{d_1 d_m} \Big/ \frac{1}{d_1^2} = P(d_m - d_1)^2 \Big/ \frac{1}{d_1^2} \tag{12}$$

As $d_1 < d_m$ and $\Gamma_m < 1$, in general we will have $\frac{1}{d_1^2} \gg \frac{\Gamma_m^2}{d_m^2}$. Here we take an approximation by letting

$$\frac{1}{d_1^2} \approx \frac{1}{d_1^2} + \sum\nolimits_{m=2}^{M} \frac{\Gamma_m^2}{d_m^2} = 2P(0)$$

Robust M-path algorithm (M is known)

Input $\hat{S}_n, C, \lambda_n$

Output d_1

1. $\mathrm{P}(k) = \sum_{n=1}^{N} \frac{\hat{S}_n}{c \cdot \lambda_n^2} \cdot e^{-i2\pi \frac{k}{N} n}, k = 1, ...N$

2. Find M largest DFT amplitudes $P_1, P_2, ..., P_M$

3. $d_1 = 1/\sqrt{P(0) - \sum_{i=1}^{M} P_i^2 / 2P(0)}$

Figure 7: Robust M-path algorithm where M is known

By this approximation, we have

$$\Gamma_m^2 / d_m^2 \approx P(d_m - d_1)^2 / 2P(0)$$

Substituting it in Eq. (9) obtains

$$\begin{aligned} d_1 &= 1/\sqrt{P(0) - \sum_{m=2}^{M} \frac{\Gamma_m^2}{d_m^2}} \\ &\approx 1/\sqrt{P(0) - \sum_{m=2}^{M} P(d_m - d_1)^2 / 2P(0)} \end{aligned} \tag{13}$$

By Lemma 3.1, we can safely assume that the top M DFT amplitudes $P_1, ..., P_M$ are all induced by the LoS and an NLoS path but not two NLoS paths. Under this assumption, we design a robust M-path algorithm in Fig. 7. In Sec. 5.3, we will bound the error introduced by this approximation.

4.3. Determination of path number M

Another critical issue is the determination of the number of paths M. In a nutshell, for each possible M value we will apply the robust M-path algorithm, evaluate the corresponding fitting error square

$$\epsilon = \sum_{n=1}^{N} \left(s(\lambda_n) - \hat{s}_n\right)^2$$

and select the one producing the minimal error.

The psudo-code of the whole algorithm with determination of M is given in

Fredi algorithm (unknown M)
Input $\hat{S}_n, C, \lambda_n$
Output d_1
1.For M=1 to a reasonably large number, say 20
2. Robust M-path algorithm to compute d_1
3. For $m = 1$ to M
4. $d_m = d_1 + \arg\limits_{k} P_m$
5. $\Gamma_m = P_m \cdot d_1 \cdot d_m$
6. End for
7. For each λ_n, compute $s(\lambda_n)$
8. Compute $\epsilon = \sum_{n=1}^{N} \left(s(\lambda_n) - \hat{s}_n\right)^2$
9.End for
10.$M = \arg\min\limits_{M}(\epsilon)$
11.Output d_1 with the corresponding M

Figure 8: Robust M-path algorithm where M is unknown

Fig. 8. In line 1, we try M from 1 to 20. It is worth noting that though in theory M can be any, in practice, it should be not too large and a reasonably large number, say 20, will work. In our experiments, M seldom exceeds five. For each M, we apply the robust DFT algorithm to compute d_1. When d_1 is available, all the other parameters d_m and Γ_m can be calculated accordingly (line 4 and 5). With all these parameters, we can reconstruct the RSS model and compute the fitting error square ϵ. The M producing the minimal fitting error will be selected and the corresponding d_1 is the final solution.

5. Analysis and Discussions

In this section, we give some analysis and discussions on Fredi. We first investigate the impact of signal modulation scheme, and demonstrate that it has no significant negative effects to our solution. We then show that certain degree of external radio interference will not severely affect our accuracy either. In the last part, we give a bound to the approximation error we introduced.

5.1. Impact of signal modulation scheme

On all above, we assume the signal modulation is simple sine wave. In real transmissions, we usually transmit modulated signals. Modulation is typically done by changing the sine wave frequency, amplitudes, or phase. This section will analyze the impact of the modulation scheme.

A first concern of the modulation scheme is that our model takes waves from all paths into account, while in practice some fraction of the waves may be the combination of only some paths. We argue that on one hand, this concern is true. On the other hand, the problematic fraction is negligibly small.

For example, suppose there are two paths and the path length difference is 4m. Suppose we are using 5.5G and the wavelength is 0.0545m. Thus there will be $4/0.0545 = 73$ periods of latency between waves of different paths. In other words, except the very beginning 73 periods and the very end 73 periods, the other parts are valid combinations from the both paths. Suppose the data rate is 100Kb, and each data bit is represented by 5.5G/100K=55K periods. For transmitting each bit, 73/55K=0.14% waves will be affected, which is negligible. As higher data rate transmission may impair the results, we suggest lower data rate when ranging.

5.2. Robustness on external interference

Till present, our methods assume that the input $\hat{S}_n$measures the signal strength from the transmitter only. In practice, the wireless spectrum, especially the ISM bands are very crowded and the RSS measurement may take radio energy of external signals (i.e., from another independent transmitter) into account. As a result, certain values in the sequence of $\hat{S}_n$may contain large errors. Fig. 11 gives an example of $\hat{S}_n$ and its P(k) with 5.1G being interfered. In the next, we will give analysis on the impact of such external interference

The external radio interference can be described using a pulse interference model, i.e.,

$$g(\lambda) = \begin{cases} a, |\lambda - \lambda_0| < \tau \\ 0, |\lambda - \lambda_0| > \tau \end{cases}$$

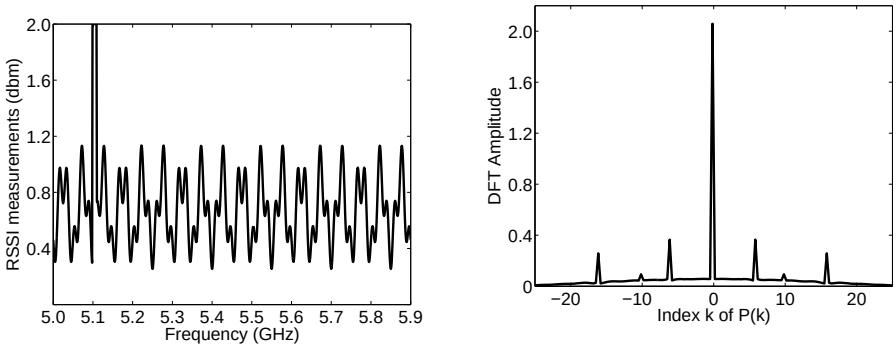

Figure 9: An example of external interference at 5.1G

where λ_0 is the central frequency of the interference radio and τ defines the range of the interference. The received signal at the receiver is the combination of $s(\lambda)$ and $g(\lambda)$. Applying the DFT method, we have

$$P'(k) = \sum_{\lambda=\lambda_1}^{\lambda_N} \frac{s(\lambda)+g(\lambda)}{c\cdot\lambda_n^2}\cdot e^{-i2\pi\frac{k}{N}n} \tag{14}$$

$$= P(K) + \sum_{\lambda=\lambda_1}^{\lambda_N} \frac{g(\lambda)}{c\cdot\lambda_n^2}\cdot e^{-i2\pi\frac{k}{N}n} \tag{15}$$

$$= P(k) + 2a\cdot\tau\cdot\sin(k)/k \tag{16}$$

where P(k) is the DFT amplitude of the original signal, and the latter part $2a\cdot\tau\cdot\sin(k)/k$ is introduced by the external interference. Noticing $\sin(k)/k$ in Eq. (16), we can find that by DFT the external interference $g(\lambda)$ is "diluted" to amplitudes near $P(0)$, and therefore its impact is effectively reduced. An example of Fredi algorithm with single external interference is shown in Fig. 9, and we will make a comprehensive investigation on the impact of external interference in Sec. 6.6.

5.3. Bounding approximation errors

In robust M-path algorithm design we take an approximation $2P(0) \approx \frac{1}{d_1^2} + \sum_{m=2}^{M}\frac{\Gamma_m^2}{d_m^2}$ to approximate $\frac{1}{d_1^2}$. In this part, we will give an analysis on the errors introduced by this approximation. Let $\hat{d}_1$ denote the real LoS path, and d_1 be the value produced by our M-path algorithm. We have the conclusion.

Theorem 5.1.

$$\frac{1}{\hat{d}_1^2} - \frac{1}{d_1^2} = \frac{(\sum_{m=2}^{M} \Gamma_m^2/d_m^2)^2}{1/d_1^2 + (\sum_{m=2}^{M} \Gamma_m^2/d_m^2)^2}$$

We omit the proof due to space limitation. As $d_1 < d_m$ and $\Gamma_m < 1$, we have $\frac{1}{d_1^2} \gg \frac{\Gamma_m^2}{d_m^2}$, and thus $\frac{1}{\hat{d}_1^2} - \frac{1}{d_1^2} \to 0$. We believe this degree of errors is acceptable and better approximation schemes are left for future work.

6. Performance Evaluations

In this section, we evaluate the performance of Fredi through experiments based on real implementation. We first introduce the experiment setup, and present the experimental results in detail.

6.1. Experiment setup

We implement the complete Fredi method using the GNU USRP2 platform [7]. We select the USRP2 platform as it provides the full control for physical layer information, which is extremely helpful to analyze the experimental data. The RFX5500 daughter boards are used to support frequency hopping from 5.0G to 5.9G. During ranging process, the transmitter sends out packets that carry the frequency hopping information. The receiver receives the packets, decodes to synchronization information, and measure the RSS of the packets in the meanwhile.

In our experiments, up to N measurements are record for one ranging process, and in later sections we will investigate the impact of N. Each RSS value is averaged from five runs, and all the data are transmitted back to a PC and processed in a centralized manner. The hardware-dependent parameters are obtained in an off-line manner. As this is a single-run operation, the overhead is acceptable and in practice, this value can be measured by the manufacturer during the hardware production. We conduct the experiments in three indoor environments, though Fredi is general enough that does not need to be indoor. As illustrated in Fig. 11, 10, 12, the three are typical office, hall, and exhibition area.

Figure 10: Hall

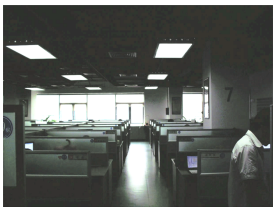

Figure 11: Office

Figure 12: Exhibition

To investigate the effectiveness of Fredi, we also implement the traditional RSS-based ranging(N=1) in the same test-bed and make comparisons with Fredi. In our designs, RSS measurements are the only input and no other information is employed. To make a fair comparison, we do not use any other information in traditional methods either. Thus, traditional RSS-based algorithms can do very little. Given the hardware-dependent parameter C as in Fredi design, we adopt the open space model (Eq. (2)) to compute the theoretical RSS, compare the measured RSS values with the theoretical ones, and map the RSS values to the corresponding distances.

In our experiments, we evaluate only one metric, ranging accuracy. Given the real distance $\hat{d}_1$, we record the measured distance d_1, and the error by comparing them.

6.2. Effectiveness of robust DFT-based algorithm

In the first set of experiments, we investigate the original M-path algorithm and the robust M-path. Notice that since we are in real environments, we have no knowledge about M. The experiments are conducted in the first "hall" environment. For each environments, we conduct experiments at three completely different positions labeled as "Position 1", "Position 2", and "Position 3".

Fig. 13 plots the ranging measurement errors against the real distance using the original M-path algorithm. We can find that there is no clear relation between the measured and real distances. We believe this is because the idealized method fully depends on the input of the third DFT amplitude

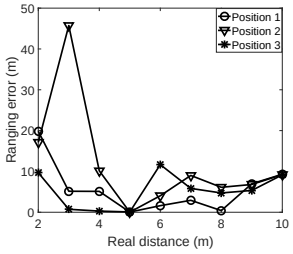

Figure 13: Ranging results of original algorithm

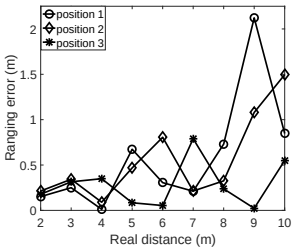

Figure 14: Fredi in hall environments

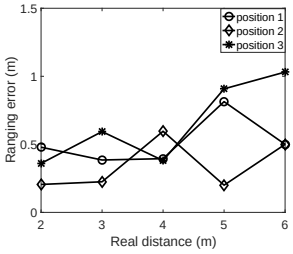

Figure 15: Fredi in exhibition environments

$P(\arg\limits_k P_1 - \arg\limits_k P_2)/(P_1 \cdot P_2)$. In practice, it can be quite small and is largely deviated from the true value due to the measurement noise and DFT leakage.

Fig. 14 shows the results by the robust M-path algorithm under the same environment. The accuracy of the ranging greatly improves compared with the original one. Within 4m, the accuracy is within 0.5m, and within 6m, the range error is no more than 1m. Beyond 9 meters, there is a sharp degradation of the accuracy to 2.2 meters. In later Sec. 7.1, we will explain why there is a sharp degradation beyond 9m. In short, the core reason is due to the imperfect antennas which will introduce the polarization problem. The consequence is that when the transmitter and receiver are set at a specific distance (9m in this case), an NLoS path will be counted as a LoS path and thus the accuracy will be significantly affected. Because of such un-expected behavior due to hardware constraint, in later we only evaluate the performance within 6m.

6.3. Impact of the changing environments

We conduct the same experiments in the other two environments and the results are shown in Fig. 15 and Fig. 16 respectively. For the "exhibition" environments, the results are similar. Within 4m, the error is about 0.5m, and within 6m, the error is about 1m. For the more complex office layout, the performance is slightly demoted. In most cases, the performance is similar to the other environments, while there is one exception. At the position 3, 4m, the ranging error is 1.3m. We believe these are again due to the imperfect antennas.

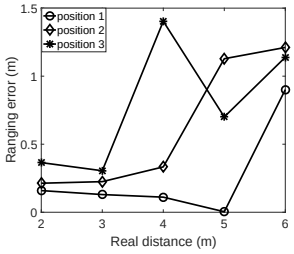

Figure 16: Fredi in office environments

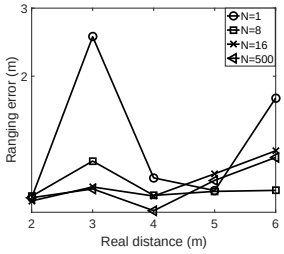

Figure 17: Impact of N in hall environments

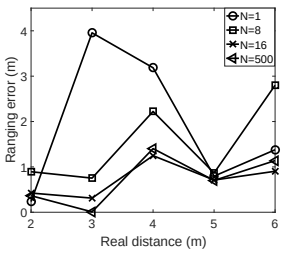

Figure 18: Impact of N in office environments

6.4. Impact of N

Different transceiver hardware may support different number of frequencies. For example, the 802.11 b/g devices support up to 13 channels (central frequencies), and TelosB sensor nodes can switch to 16 frequencies. In this part, we investigate the impact of the number of measurement N on the ranging accuracy and all the three environments are investigated. Notice that when $N = 1$, it becomes the traditional method of no frequency diversity being exploited.

Fig. 17, 18, 19 investigate the impact of N on ranging performance for different environments. We vary $N = 1$ to $N = 500$. For ease of presentation, we only show some representative results. Fig. 17 is for the "hall" environment where the multipath effect is not as severe as the other two. From the results, we find that when N is less than 16, the ranging error is quite high, and more importantly, the measured distance is not a monotonic function of the real distance. Such performance can hardly be accepted in practice. For scenarios of $N \geqslant 16$, the performance greatly improves. We further notice that there is not a great incentive to further increase N. The performance gap between $N = 16$ and $N = 500$ is less than 10 percent. Similar results are observed in the other two environments as shown in Fig. 18 and 19.

6.5. Comparisons with traditional methods

In this part, we make comparisons between Fredi and the traditional RSS-based ranging. We implement the traditional RSS ranging as Sec. 6.1 described.

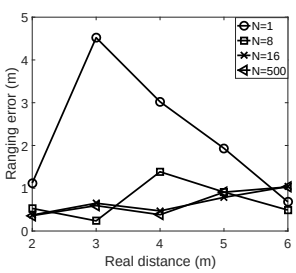

Figure 19: Impact of N in exhibition environments

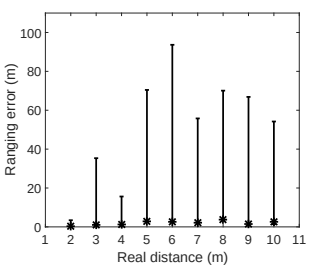

Figure 20: Traditional RSS ranging in hall

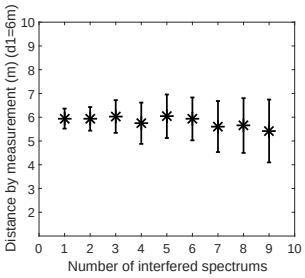

Figure 21: Impact of external radio interference

Fig. 20 shows the ranging accuracy of traditional RSS in the same hall environment. For each setup, we use an errorbar to depict all the results.

We observe that when the transmitter and receiver are very close to each other, i.e., $d_1 = 2$, traditional methods can perform pretty well. The ranging accuracy is within 1m and the results are very stable. This is because in this close distance, the LoS path waves will exhibit preeminent advantages by its shorter length and no reflection lose. In addition, at this distance, there are not too many, if any, NLoS paths, and thus the impact of multipath effect is little. Beyond three meters, the advantages of LoS path waves becomes weakened, and more NLoS paths appear. Consequently, the ranging errors sharply increase and performance fluctuate dramatically. At three meters, the measured distance error ranges from 0.06m to 38.33m. Notice that our experiments are conducted in the daily office environment (you can see a person passing through our test-bed in pic. 11), the environment is keep changing and the multi-paths are dynamically generated and disappear, and thus the raw RSS fluctuate dramatically. As the distance further increases, the performance of traditional methods further degrade. We even observe a measured distance error as 96m when the real distance is only 6m. Besides this exceptional errors, the other results are similar regardless the read distance.

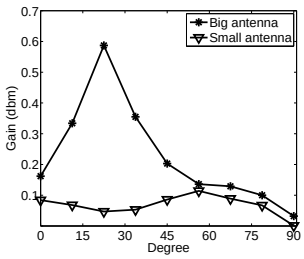

Figure 22: Antenna gains at different directions

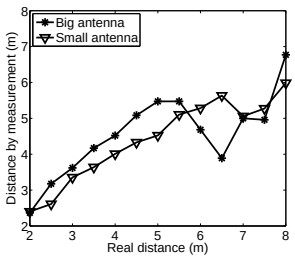

Figure 23: Fredi in exhibition environments

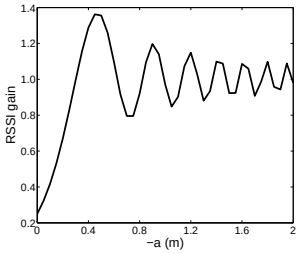

Figure 24: Antenna gain with Huygens effect

6.6. Impact of the external interference

In Sec. 5.2, we investigate the robustness of our Fredi algorithm against the external radio interference. Besides the transmitter and receiver, we setup other USRP devices to generate external interference and up to 9 frequencies are interfered. The selection of the interfered spectrum is random with all results reported. The number of interfered spectrums varies from 1 to 9. The transmission frequency is from 5.0G to 5.9G. Every interference has 30M band. The real distance between the transmitter and receiver is fixed to 6m and results are shown in Fig. 21 with error bars.

Clearly the external radio interference greatly deteriorates the accuracy of the RSS-based ranging. We believe more affected channels will further impair the accuracy and more robust designs are left for future work.

7. Discussions

In this section, we discuss some more practical issues for RSS-based ranging.

7.1. Antenna polarization

In this section, we explain why the performance becomes un-stable beyond 7m. A critical assumption in our work is that the antenna is omni-directional. Under this assumption, since LoS path has the largest amplitude. In practice, however, this is not always true as antennas are always directional. Waves emitted out of certain directions are stronger than other directions. Consequently a

NLoS path wave, when it is along the antenna-favored direction, may stronger than the LoS one.

Figure 22 shows the antenna gain of two antennas we have use, a big one with larger gain and a small one with less gain. The x-axis is the direction and the y-axis is the antenna gain along the direction. We can find that the big antenna has the largest gain at 20 degree, and the difference between different directions is up to 12 times. An NLoS path wave omitted through 20 degree is very possible to exceed the LoS path wave, and thus is falsely treated as the LoS path.

Yet we have no solutions for antenna polarization, we adopt a small antenna in our experiments. It performs much better than the big one, though it is still not a perfect omni-directional antenna. Ranging results with these two antennas are depicted in Fig. 23.

7.2. Huygens Effect

Similar to the light, the electromagnetic wave also has an ability to diffract. When the sender and receiver are both too near to the ground, the so-called Huygens effect will appear and the energy model in Eq. (eq1) will fail and we can only adopt Eq. (17). Let $k = \sqrt{\frac{2}{r\lambda}}$, and we have

$$\begin{cases} Q_1(ka) = \int_0^{ka} \cos\frac{\pi u^2}{2} du \\ Q_2(ka) = \int_0^{ka} \sin\frac{\pi u^2}{2} du \end{cases} \tag{17}$$
$$s_a = \frac{1}{2} s\{[\frac{1}{2} - Q_1(ka)]^2 + [\frac{1}{2} - Q_2(ka)]^2\}$$

where s is the Eq. (2) by open space model. Figure 24 shows the antenna gain at different heights by Hugyens model Eq. (17), and Fig. 25 shows the ranging results with different heights. As we typically have no knowledge on the conductivity of the land, the ranging behavior near ground is hard to predict. We therefore suggest that in the indoor environment, ranging should be done for positions above 1m.

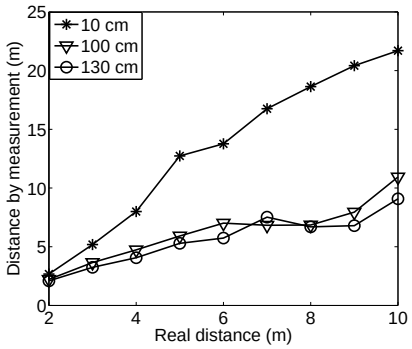

Figure 25: Ranging with Huygens effect

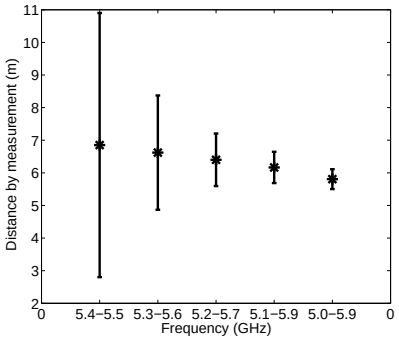

Figure 26: Impact of close paths with respect to supported frequencies

7.3. Impact of close paths

In practice, we can only measure a limited number of different frequency RSS. We thus have a limited capability for the DFT. Notice that when two paths are very close to each other, by Eq. (7) DFT-method may not be able to distinguish they two, resulting large errors. This is particularly true for NLoS paths being close to the LoS one.

To investigate the impact of close paths in practice, we set LoS path as 6m and the NLoS path as 6.5m by placing a metal object nearby. We vary the scanned frequency as Fig. 26 x-axis indicates. We can find that increasing range of the frequency can effectively address the problem. When only 0.1G spectrum is scanned, the range error is huge, and when more are allowed, say from 5.2 to 5.7, it is with 2.2m. When 5.0-5.9 is allowed, it is with 0.5m. We further vary the NLoS path from 6m to 8m by setting a metal object near the LoS path. The results are shown in Fig. 26. From the figure, we can see expand the range of the measurement frequency the measurement error will be smaller.

7.4. Changing Environment

Changing environment is one of hard problems in RSS-based localization method. For example, in fingerprint based methods [2] [8], a radio map should be updated by costly human labor works whenever environment is changed. For

example, moving people, closing a door and moving a cup may cause the indoor environment changing.

This changing environment can induce dynamic multi-path effect. If Fig. 6(a) is derived from a changing environment to indicate the multi-path effect, the measurements would get changed over time. However, the time it takes to compute RSS (milliseconds), in theory, is much shorter than the time between the movements of humans. We can consider that at one point, the environment and multi-path effect are static. Fredi can use multiple frequencies on this one time point to compute the distance. Therefore, changing environment has no effect on Fredi.

7.5. Limitations

Fredi does not support transition or attenuation in the propagation medium through walls. Therefore, Fredi cannot measure the distance for a target behind a wall. To address this problem, we can leverage the idea of finger-print-based methods to measure the distance through the wall. Second, we discuss the antenna polarization problem (Section 7.1) but yet have no clear solutions to deal with it. Third, the close paths problem (Section 7.3) and the Huygens effect problem (Section 7.2) can only be alleviated by using some practical methods. For example, the anchor may not be placed on the floor.

7.6. Scalar Power

There are some others effects of electromagnetic propagation, which are not possible to capture by received scalar Power values only, such as transmission time, Angle-of-Arraival, interferometric geolocation, and doppler effects. Some of them can be used in indoor localization (Discussed in Section 8). However, these methods often require special or expensive hardware. For example, Time-of-Arrival [9] utilizes transmission time to compute the distance. In the indoor environment, from anchor to target, the distance is short as meters in majority cases. Therefore, transmission time is too short to be measured by a commonly used business equipment — customized equipment will be needed.

As part of the future work, we may improve Fredi accuracy by using existing methods, which are not scalar power based (e.g., TODA). The exploration of new feature of electromagnetic propagation is also a good direction for indoor localization.

8. related work

RSS-based ranging has been an active research area for decades of years. Because of the multi-path and many other practical issues, the RSS cannot be simply converted to the ranging and various techniques have been proposed. We classify the existing methods into two categories, namely model-based and fingerprint-based.

In the model-based approaches, a radio propagation model is established to predict the RSS at the different distances. As the simple radio propagation model performs badly in practice, various new models have been proposed. For example Lim et al. [10] used the LDPL model, and ARIADNE [11] adopted a ray-tracking model based on floor maps. In these works, the more inputs for building models were obtained a larger deployment of measurement nodes (e.g., AP). As the model parameters are quite different for differen nodes, these approaches are limited in dynamic environments. None of them exploited the frequency diversity yet.

In the fingerprint-based approaches (e.g., RADAR [2] and PinLoc [8]), an RF signal map is build in a pre-deployment stage. Users match the measured RSS with this map to obtain their locations. LANDMARC [12] localizes nodes by finding some reference nodes who has the similar RSS with the target nodes. Besides these deterministic approaches, probabilistic approaches are also proposed such as [13, 14, 15, 16, 17]. For example, Horus employs a stochastic model to describe the RSS map and adopt a maximum likelihood based approach. Ambience information can also be used to build the fingerprint [18]. Fingerprint-based approaches can effectively address the multipath issue but are limited to static environments where the environment parameters do not change.

In dynamic environments, e.g., people are moving around causing more radio paths, the fingerprint may fail to capture the location features. In that scenario, the map has to be rebuild, which is often too costly. Coarse grained map [19] can cut down the pre-deployment overhead, while the efforts are still substantial and the cost is the ranging accuracy. Zee localization [20] is a fingerprint-based approach. It uses smartphones and places to match user paths into an indoor map. There are some constrains on the map, such as wall and barrier. For example, people cannot pass through a wall. Based on these constrains, Zee can achieve more accurate localization. LiFS [21] was developed for wireless indoor localization using smartphone-based crowdsourcing. LiFS estimates a RSS map in user traces using inertial sensors. AcMu [22] can automatically update wireless indoor RSS map by exploiting the static behaviors of users' mobile devices. These approaches require recording RSS values into a RSS map and maintaining the map in the presence of environment changes. In contrast, Fredi does not require human participation for creating the RSS map or additional effort for maintaining the map.

In addition to RSS-based ranging, which uses scalar power of electromagnetic propagation, there are some other indoor ranging techniques using other features of electromagnetic propagation, such as Angle-of-Arrival (AoA)[23][24], Time-of-Arrival[9] [25][26][27], Time-Difference-of-Arrival [28][29], light-based [30], interferometric geolocation [31], and Doppler effects [32]. These approaches are always based on the assumption of single LoS path and they often requires special hardware to obtain the required information. Interestingly, some recent works uses the common-off-the-shelf hardware to realize the above principles. For example, Borealis [33] is AoA-based but finds the direction of an AP by rotating the receiver around a signal blocking object. SpinLoc [34] extracts the physical layer information provided by hardware driver to get the direction information. To the contrast, Fredi does not require any special hardware, physical layer information, or interactions from the users. All operations are done in a automatic and user-transparent manner.

A very important related work is proposed by Rallapalli et.al [35]. They

noticed the frequency diversity of RSS measurement but simply used the average to represent the RSS. In fact, all the RSS values at the different frequencies are correct. The difference exists because of the wave phases. Another similar work is done by Zhang et.al [36] which formulates the problem as a non-linear optimization problem. They solve the problem with very strict constrains and thus can be applied in very limited scenairos. The third important related work is proposed by Wu et.al [37] which also explore a method to overcome the multi-path effect. They need more information extracted from physical layer besides RSS. Special hardwares are needed at the receiver.

9. Conclusion and Future Work

Frequency diversity provides a powerful tool to address the multipath effect and the radio interference. By frequency diversity, RSS measurements at different frequencies will be fundamentally different, which help us to build a mathematical model to figure out all the dynamic factors. Compared with the traditional methods to deal with multipath effect and radio interference, Fredi is simple and easy to employ. The only input is the RSS measurement, no physical layer information is needed, and no cooperation between nodes are needed. The only requirement is to quick measure the RSS at different frequencies so that the dynamic factors will not likely to change during the measurement. By current off-the-shelf hardware, this is a reasonable requirement. Experimental results show that attractive performance of Fredi. In all three environments, the ranging error is consistently no more than 0.5m within 4m and no more than 1m within 6m, compared with the traditional method of up to 100m in the same environment.

The work can be carried on along the following directions. First, we will implement Fredi using hardware platform rather than USRP-2 and build a localization and tracking system. Second, we discuss the antenna polarization problem but yet have no clear solutions to deal with it. Third, we will alleviate the negative impact of Huygens effect. Forth, we attempt to address the

limitations of the hardware when different paths are very close. Fifth, ranging without line of path is a problem that needs to be solved in Fredi. The idea of finger-print-based methods is a potential solution. Finally, some other features besides the scalar power of electromagnetic propagation may be used to help improve the accuracy of Fredi.

10. Proof of the Equation(8)

$$
\begin{aligned}
s(\lambda) &= \lambda^2 \cdot \sum_{t=1}^{N} \frac{\left(E_1(t) + E_2(t) + E_3(t) + ... + E_n(t)\right)^2}{N} \\
&= C \cdot \lambda^2 \cdot \sum_{t=1}^{N} \frac{(\frac{\lambda}{d_1}\sin(\frac{2\pi c}{\lambda}t) + \sum_{s=2}^{n}\frac{\lambda}{d_2}\Gamma_s \sin(\frac{2\pi c}{\lambda}t + \frac{d_1-d_s}{\lambda}\cdot 2\pi)}{N} \\
&+ 2\sum_{i=1}^{n}\sum_{j=1}^{n} \frac{\frac{\lambda}{d_i}\Gamma_i \sin(\frac{2\pi c}{\lambda}t + \frac{d_1-d_i}{\lambda}\cdot 2\pi)\cdot \frac{\lambda}{d_j}\Gamma_j \sin(\frac{2\pi c}{\lambda}t + \frac{d_1-d_j}{\lambda}\cdot 2\pi)}{N} \\
&\because \frac{1}{N}\sum_{t=1}^{N}\frac{\lambda^2}{d^2}\sin^2(wt+\psi) = \frac{\lambda^2}{2d^2} \\
&\because \sin(wt)\cdot\sin(wt+\psi) = \frac{\cos(\psi) - \cos(2wt+\psi)}{2} \\
&\because \frac{1}{N}\sum_{t=1}^{N}\cos(t) = 0 \\
&\therefore s(\lambda) = C\cdot\lambda^2\cdot(\sum_{t=1}^{N}\frac{\Gamma_n}{2d_m^2} + \sum_{m\neq m'}\frac{\Gamma_m\Gamma_{m'}}{d_m d_{m'}}\cos(\frac{d_m - d_{m'}}{\lambda}))
\end{aligned}
\tag{18}
$$

References

[1] Z. Yang, Y. Liu, Quality of trilateration: Confidence-based iterative localization, IEEE TPDS 21 (5) (2010) 631–640.

[2] P. Bahl, V. Padmanabhan, Radar: An in-building rf-based user location and tracking system, in: Proc. of IEEE INFOCOM, Ieee, 2000.

[3] Y. Shu, Y. Huang, J. Zhang, P. Coué, P. Cheng, J. Chen, K. G. Shin, Gradient-based fingerprinting for indoor localization and tracking, in: INFOCOM, 2014.

[4] H. Rahul, F. Edalat, D. Katabi, C. Sodini, Fara: Frequency-aware rate adaptation and mac protocols, in: Proc. of ACM MOBICOM, ACM, 2009, pp. 193–204.

[5] J. G. Proakis, D. G. Manolakis, Digital signal processing, Pearson Education, 2013.

[6] F. Harris, On the use of windows for harmonic analysis with the discrete fourier transform, Proc. of the IEEE 66 (1) (1978) 51–83.

[7] E. R. LLC, Universal soft radio peripheral (2006).
URL http$\protect\kern+.2222em\relax$//www.ettus.com/

[8] S. Sen, B. Radunovic, R. Choudhury, T. Minka, Precise indoor localization using phy layer information.

[9] C. Peng, G. Shen, Y. Zhang, Y. Li, K. Tan, Beepbeep: a high accuracy acoustic ranging system using cots mobile devices, in: Proc. of ACM Sensys, ACM, 2007, pp. 1–14.

[10] H. Lim, L. Kung, J. Hou, H. Luo, Zero-configuration, robust indoor localization: Theory and experimentation, in: Proc. of IEEE Infocom, Ieee, 2006, pp. 1–12.

[11] Y. Ji, S. Biaz, S. Pandey, P. Agrawal, Ariadne: a dynamic indoor signal map construction and localization system, in: Proc. of ACM Mobisys, ACM, 2006, pp. 151–164.

[12] L. M. Ni, Y. Liu, Y. C. Lau, A. P. Patil, Landmarc: Indoor location sensing using active rfid, in: Proc. of IEEE PerCom, 2003.

[13] M. Youssef, A. Agrawala, The horus wlan location determination system, in: Proc. of ACM Mobisys, 2005.

[14] A. Haeberlen, E. Flannery, A. M. Ladd, A. Rudys, D. S. Wallach, L. E. Kavraki, Practical robust localization over large-scale 802.11 wireless networks, in: Proc. of ACM MobiCom, 2004.

[15] A. Ladd, K. E. Bwkris, A. Rudys, Robotics-based location sensing using wireless ethernet, in: Proc. of ACM MobiCom, 2002.

[16] T. Tonteri, A statistical modeling approach to location estimation, in: IEEE Transaction on Mobile Computing, 2002.

[17] M. A. Youssef, A. Agrawala, A. U. Shankar, Wlan location determination via clustering and probability distributions, in: Proc. of IEEE PerCom, 2003.

[18] M. Azizyan, I. Constandache, R. Roy Choudhury, Surroundsense: mobile phone localization via ambience fingerprinting, in: Proc. of ACM MOBICOM, ACM, 2009, pp. 261–272.

[19] A. Haeberlen, E. Flannery, A. Ladd, A. Rudys, D. Wallach, L. Kavraki, Practical robust localization over large-scale 802.11 wireless networks, in: Proc. of ACM MOBICOM, ACM, 2004, pp. 70–84.

[20] A. Rai, K. K. Chintalapudi, V. N. Padmanabhan, R. Sen, Zee: Zero-effort crowdsourcing for indoor localization, in: Proceedings of the 18th annual international conference on Mobile computing and networking, ACM, 2012, pp. 293–304.

[21] C. Wu, Z. Yang, Y. Liu, Smartphones based crowdsourcing for indoor localization, IEEE Transactions on Mobile Computing 14 (2) (2015) 444–457.

[22] C. Wu, Z. Yang, C. Xiao, Automatic radio map adaptation for indoor localization using smartphones, IEEE Transactions on Mobile Computing 17 (3) (2018) 517–528.

[23] P. Rong, M. Sichitiu, Angle of arrival localization for wireless sensor networks, in: Proc. of IEEE SECON, Vol. 1, Ieee, 2006, pp. 374–382.

[24] M. Kotaru, K. Joshi, D. Bharadia, S. Katti, Spotfi: Decimeter level localization using wifi, in: Proceedings of the 2015 ACM Conference on Special Interest Group on Data Communication, ACM, 2015, pp. 269–282.

[25] D. Vasisht, S. Kumar, D. Katabi, Decimeter-level localization with a single wifi access point, in: 13th USENIX Symposium on Networked Systems Design and Implementation (NSDI 16), 2016, pp. 165–178.

[26] A. Savvides, C. Han, M. Strivastava, Dynamic fine-grained localization in ad-hoc networks of sensors, in: Proc. of ACM Mobicom, ACM, 2001, pp. 166–179.

[27] B. Kusy, P. Dutta, P. Levis, M. Maroti, A. Ledeczi, D. Culler, Elapsed time on arrival: a simple and versatile primitive for canonical time synchronisation services, IJAHUC 1 (4) (2006) 239–251.

[28] N. Priyantha, A. Chakraborty, H. Balakrishnan, The cricket location-support system, in: Proc. of ACM Mobicom, ACM, 2000, pp. 32–43.

[29] A. Smith, H. Balakrishnan, M. Goraczko, N. Priyantha, Tracking moving devices with the cricket location system, in: Proc. of ACM Mobisys, ACM, 2004, pp. 190–202.

[30] R. Stoleru, T. He, J. A. Stankovic, D. Luebke, A high-accuracy, low-cost localization system for wireless sensor networks, in: Proceedings of ACM SenSys, 2005.

[31] M. Maroti, B. Kusy, G. Balogh, P. Volgyesi, A. Nadas, K. Molnar, S. Dora, , A. Ledeczi, Radio interferometric geolocation, in: Proceedings of ACM SenSys, 2005.

[32] B. Kusy, A. Ledeczi, X. Koutsoukos, Tracking mobile nodes using rf doppler shifts, in: Proc. of ACM Sensys, ACM, 2007, pp. 29–42.

[33] Z. Zhang, X. Zhou, W. Zhang, Y. Zhang, G. Wang, B. Zhao, H. Zheng, I am the antenna: accurate outdoor ap location using smartphones, in: Proc. of ACM Mobicom, ACM, 2011, pp. 109–120.

[34] H. Chang, J. Tian, T. Lai, H. Chu, P. Huang, Spinning beacons for precise indoor localization, in: Proc. of ACM Sensys, ACM, 2008, pp. 127–140.

[35] S. Rallapalli, L. Qiu, Y. Zhang, Y. Chen, Exploiting temporal stability and low-rank structure for localization in mobile networks, in: Proc. of ACM MobiCom, 2010.

[36] D. Zhang, Y. Liu, X. Guo, M. Gao, L. Ni, On distinguishing the multiple radio paths in rss-based ranging, in: Proc. of IEEE INFOCOM, 2012, 2012.

[37] C. Wu, Z. Yang, Z. Zhou, K. Qian, Y. Liu, M. Liu, Phaseu: Real-time los identification with wifi, in: Computer Communications (INFOCOM), 2015 IEEE Conference on, IEEE, 2015, pp. 2038–2046.